



Originally published as:

Neri, M., Rivalta, E., Maccaferri, F., Acocella, V., Cirrincione, R. (2018): Etnean and Hyblean volcanism shifted away from the Malta Escarpment by crustal stresses. - *Earth and Planetary Science Letters*, 486, pp. 15–22.

DOI: <http://doi.org/10.1016/j.epsl.2018.01.006>

1 Etnean and Hyblean volcanism shifted away from the Malta
2 Escarpment by crustal stresses

3 **Marco Neri^{1*}, Eleonora Rivalta², Francesco Maccaferri², Valerio Acocella³, Rosolino**
4 **Cirrincione⁴**

5 ¹ *Istituto Nazionale di Geofisica e Vulcanologia, Sezione di Catania, Osservatorio Etneo, Piazza*
6 *Roma 2, 95125, Catania, Italy*

7 ² *GFZ German Research Center for Geosciences, Potsdam, Germany*

8 ³ *Dipartimento Scienze Roma Tre, Roma Italy*

9 ⁴ *Dipartimento di Scienze Biologiche, Geologiche e Ambientali – Università di Catania. C.so*
10 *Italia 57, 95129 Catania*

11 *Corresponding author

12 **Key words**

13 Intraplate volcanism, fault scarp, dike propagation, Malta Escarpment, Hyblean volcanism, Etna.

14 **ABSTRACT**

15 A fraction of the volcanic activity occurs intraplate, challenging our models of melting
16 and magma transfer to the Earth's surface. A prominent example is Mt. Etna, eastern Sicily,
17 offset from the asthenospheric tear below the Malta Escarpment proposed as its melt source. The
18 nearby Hyblean volcanism, to the south, and the overall northward migration of the eastern
19 Sicilian volcanism are also unexplained. Here we simulate crustal magma pathways beneath
20 eastern Sicily, accounting for regional stresses and decompression due to the increase in the
21 depth of the Malta Escarpment. We find non-vertical magma pathways, with the competition of
22 tectonic and loading stresses controlling the trajectories' curvature and its change in time,
23 causing the observed migration of volcanism. This suggests that the Hyblean and Etnean
24 volcanism have been fed laterally from a melt pooling region below the Malta Escarpment. The
25 case of eastern Sicily shows how the reconstruction of the evolution of magmatic provinces may

26 require not only an assessment of the paleostresses, but also of the contribution of surface loads
27 and their variations; at times, the latter may even prevail. Accounting for these competing
28 stresses may help shed light on the distribution and wandering of intraplate volcanism

29

30 **1. INTRODUCTION**

31 The distribution of volcanoes on the Earth's surface is determined by two main factors:
32 the availability of melt at depth, generally associated with the decompression of mantle or crustal
33 material, and the presence of a pathway for magma to ascend to the surface, controlled by
34 lithospheric discontinuities or crustal stresses enhancing dike propagation and ascent. Intraplate
35 volcanism is especially challenging to explain. The debate focuses on both the melting
36 mechanisms and magma availability at a more regional scale (Tang et al., 2014), as well as the
37 crustal magma pathways and their controlling features (Shabanian et al., 2012). The Etnean and
38 Hyblean volcanism in eastern Sicily (Fig. 1) provides an exemplary case to investigate these
39 processes at the crustal scale.

40 Mt. Etna is the site of sustained volcanism whose composition, similar to that of Ocean Island
41 Basalts (OIB; Niu et al., 2011), has traditionally been ascribed to decompression of mantle
42 material upwelling under extension (Barberi et al., 1973) or the presence of a plume (Tanguy et
43 al., 1997). More recently, decompression melting related to suction or toroidal return flow
44 sideways of the subduction underneath the Calabrian Arc has been suggested as an alternative to
45 the plume hypothesis (Gvirtzman and Nur, 1999; Doglioni et al., 2001; Schellart, 2010;
46 Faccenna et al., 2011), or in interaction with it (Schiano et al., 2001), to explain the
47 compositional changes over time. The ascent pathway is widely identified in a lithospheric
48 discontinuity to the east of Etna, the Malta Escarpment (Corsaro et al., 2002; Siniscalchi et al.,
49 2012; Polonia et al., 2016). However, this latter hypothesis does not explain why Mt. Etna has
50 developed on the footwall of, and not directly on, the Malta Escarpment (ME) itself. The earlier
51 Hyblean volcanism, scattered to the south of Etna, is also located in the foreland, further away

52 from the Malta Escarpment. Compositionally, the Hyblean volcanism is similar to OIB and
53 highly similar to the earliest Etnean volcanism, lacking the transitional components to arc
54 volcanism that some researchers identify for Etna (Tanguy et al., 1997); unlike to the Etnean
55 volcanism, the Hyblean volcanism does not show any significant trend of magmatic
56 differentiation (Beccaluva et al., 1998; Schiano et al., 2001; Manuella et al., 2013). The Hyblean
57 volcanism has been generically linked to extensional tectonics (Barberi et al., 1973) or to a deep-
58 rooted mantle plume (Tanguy et al., 1997; Schiano et al., 2001). The Hyblean and Etnean
59 magmas are spatially continuous to the west of the Malta Escarpment, as demonstrated by
60 outcrops, boreholes and seismic reflection lines (Torelli et al., 1998; Branca et al., 2011).
61 However, the compositional and spatial continuity of the Hyblean and Etnean volcanism, as well
62 as its overall northward migration subparallel to, but offset from, the Malta Escarpment, are still
63 unexplained.

64 Magma is predominately transported through the crust via magma-filled fractures, or dikes,
65 propagating by hydraulic fracturing (Rubin, 1995). Dikes tend to follow trajectories
66 perpendicular to the least compressive principal stress, σ_3 (Dahm, 2000), thus being very
67 sensitive to the crustal state of stress. Heterogeneous crustal stresses may drive dike propagation
68 through curved or anyway complex pathways (Dahm, 2000; Roman and Jaupart, 2014;
69 Sigmundsson et al., 2015;). In particular, the distribution of surface loads may exert a major
70 control on crustal stress (Dahm, 2000; Watanabe et al., 2002). If surface loads are not evenly
71 distributed (e.g. if there are volcanic edifices and fault scarps) magma pathways may bend,
72 reaching the surface offset up to several tens of km from the melt pooling zone (Watanabe et al.,
73 2002; Maccaferri et al., 2014). Here we test the hypothesis that the significantly asymmetric
74 distribution of loads across the Malta Escarpment may have been responsible for bending dike
75 trajectories towards the fault footwall. We combine for the first time two separate notions: that
76 observations of surface volcanism (vent location and fissure orientation) are indicative of
77 paleostresses, and that elastic stresses due to gravitational loads may play a role and at times

78 even dominate over tectonic contributions (e.g. in case of major topographic or bathymetric
79 variations). Based on this approach to evaluate stresses, we constrain the location of Etnan and
80 Hyblean melt source by backtracking the simulated dike trajectories from the observed eruptive
81 locations down to the Moho.

82

83 **2. TECTONIC SETTING AND VOLCANISM**

84 The Malta Escarpment, a regional NNW-SSE trending fault system offshore eastern
85 Sicily, separates the thinner Ionian oceanic lithosphere subducting beneath the Calabrian Arc (to
86 the east) from the thicker continental crust of the African foreland (to the west) (Fig. 1). The
87 Malta Escarpment probably activated since Mesozoic, even though its main faulting event
88 occurred in the Neogene (Upper Miocene; Argnani and Bonazzi, 2005). The ~350 km² wide
89 scattered volcanic activity in the Hyblean region has involved four main cycles since the Upper
90 Triassic, the latter occurring in the Upper Miocene–Lower Pleistocene (1-10 Ma; Patacca et al.,
91 1979; Carbone et al., 1987; Beccaluva et al., 1998; Manuella et al., 2013). Over these cycles,
92 volcanism in the Hyblean foreland migrated northwestward (Fig. 2). Westward migration of the
93 eruptive vents during the Plio-Pleistocene was accompanied by 90° rotations in the alignment of
94 the eruptive fissures, activating NE-SW to ENE-WSW trending dextral to normal faults, (SG and
95 LSG in Fig. 2), suggesting the tectonic regime became compressive (Ghisetti and Vezzani, 1980;
96 Grasso et al., 1991; Beccaluva et al., 1998). Such an overall E-W compression may have
97 continued until ~0.85 Ma (Catalano et al., 2008), or was replaced by neutral tectonic conditions
98 (Cultrera et al., 2015), anticipating the E-W extension from ~0.85 Ma until the present (Catalano
99 et al., 2008; Montone et al., 2012; Cultrera et al., 2015).

100 Volcanic activity in the Hyblean foreland terminated at ~1.4 Ma (Torelli et al., 1998) and
101 then focused in the Etna area during the last 0.5 Ma. Therefore, this change from compression to
102 extension in the Hyblean foreland seems associated with the northward migration of volcanism
103 towards the Etna area. Such a coexistence of volcanism with compression and its migration at

104 the onset of extension is not straightforward and deserves an appropriate tectono-magmatic
105 model.

106 The first period of volcanism in the Etna area (600-250 ka) involved mainly tholeiitic and
107 transitional to Na-alkaline magmas, forming both sub-volcanic bodies and lava flows emplaced
108 in submarine/subaerial environment along fissures or from minor cones (Corsaro et al., 2002;
109 Branca et al., 2011). Between 225 and 142 ka, eruptions occurred mostly from fissures forming a
110 ~N-S trending edifice, producing most of the lavas presently outcropping along the Timpe Fault
111 System, the onland surface expression of the Malta Escarpment on the distal eastern flank of
112 Etna (Chiocci et al., 2011; Siniscalchi et al., 2012; Catalano et al., 2013). During the last 110 ka,
113 the fissural volcanic activity became central; the major eruptive axes migrated westward,
114 building strato-volcanoes up to 3800 m high, between 110 and 15 ka. The volcano today, 3,324
115 m high, uses the same central conduit that has been active over the last 65 ka (Branca et al.,
116 2011). Mt. Etna has been undergoing an overall ~E-W trending extension (Catalano et al., 2013)
117 associated with the activity of the Malta Escarpment (Monaco et al., 1997; Siniscalchi et al.,
118 2012; Mattia et al., 2015) and/or to N-S trending regional compression due to the southward
119 propagation of the Apenninic Chain (Lanzafame et al., 1997; Billi et al., 2010).

120 3. METHODS

121 We use a boundary element numerical code for dike propagation (Maccaferri et al., 2011)
122 based on Dahm (2000). Dikes are boundary-element pressurised cracks in 2D (plane strain).
123 Dike trajectories are computed by maximising the elastic and gravitational energy release on
124 incremental elongations of a magma filled fracture in different directions. The dikes propagate
125 upwards due to buoyancy: here the density of magma is set to 2300 kg m^{-3} while the density of
126 the host rock is 2600 kg m^{-3} . We consider three snapshots for the early development of the
127 Etnean and three for the Hyblean magmatism, respectively, based on the geologic history of the
128 area. For each snapshot, we reconstruct the scarp height and distribution of surface loads. We

129 next derive the induced crustal stresses based on analytical formulas for the stress change
 130 induced in an elastic half-space by a vertically oriented force (Davis and Selvadurai, 1996;
 131 Roman and Jaupart, 2014). Finally, we superpose tectonic extension or compression, as
 132 appropriate.

133 The intensity of the unloading pressure due to the creation of the scarp bathymetric
 134 depression, P^U , is $\Delta\rho gh$, where $\Delta\rho$ is the rock density, ρ_r , minus the density of water, ρ_w (this
 135 accounts for the load of the water column above the hanging wall of the Malta Escarpment), g is
 136 the acceleration due to gravity, and h is the topography height along profiles perpendicular to the
 137 Malta Escarpment through Etna (profile 1) or through the Hyblean foreland (profile 2). Finally,
 138 we superpose tectonic extension or compression, as appropriate. We adopt a reference frame
 139 with the y-axis oriented along the ME, the x-axis perpendicular to it and the z-axis pointing
 140 downward. In such a reference frame, the total stress tensor acting within the crust (σ^{tot}_{ij}) is the
 141 superposition of an isotropic lithostatic state of stress (with lithostatic pressure $P^L = \rho_r gz$), the
 142 stress change induced by unloading forces applied at the Earth's surface (σ^U_{ij}), reported e.g. by
 143 Dahm (2000) or Watanabe et al. (2002), and a horizontal tectonic extension (σ^T), acting
 144 uniformly through the crust. Thus:

$$145 \quad \sigma^{tot}_{ij} = P^L \delta_{ij} + \sigma^U_{ij} + \sigma^T_{ij}, \quad (1)$$

146 where $\delta_{ij} = 1$ if $i=j$ and 0 if $i \neq j$, and the only non-zero component of the tectonic stress
 147 tensor, σ^T_{ij} , is $\sigma^T_{xx} = \sigma_T$. We use $\sigma^T = 5$ MPa and -5 MPa for horizontal extension and compression,
 148 respectively, and $\sigma^T = 1$ MPa for weaker.

149 After calculating magma trajectories, we select those that emerge at locations of observed
 150 volcanism, at distance x_{vol} from the ME, and follow them backwards, until we reach a depth of
 151 30 km. There, the trajectory will be at distance x_{mag} from the ME. Since our model is elastic, we
 152 cannot extend our trajectory analysis into the Earth's mantle. For Etna, the deepest extent of our
 153 domain, the crust-mantle boundary, coincides with a magma storage region, as constrained by
 154 geochemistry (Tanguy et al., 1997; Schiano et al., 2001; Doglioni et al., 2001; Clocchiatti et al.,

155 2004). For the Hyblean magma, while there is evidence for a source between 30-80 km of depth,
156 there is no evidence for a magma storage region at the mantle-crust boundary (Beccaluva et al.,
157 1998). This means that for Etna we may be able to locate the magma storage region in (x,y,z) by
158 crossing our trajectories with the petrology information. As for the Hyblean magma, its
159 chemistry does not require a storage region, and the melt source is deeper than our modeling
160 domain. However, crustal pathways simulated down to 30 km depth may still provide important
161 constraints on the melt source.

162 As for profile 1 (Etna, Fig. 3), we consider three snapshots ($t_1=100$ ka, $t_2=250$ ka and
163 $t_3=500$ ka). We retrieve the correspondent bathymetric profiles by first removing the edifice of
164 Mt. Etna (we keep a dashed topographic profile for Mt. Etna in all figures for reference) and then
165 correcting the current Malta Escarpment bathymetry (height difference ~ 1700 m, width ~ 20 km,
166 fault dip $\sim 60^\circ$) based on information on recent slip and sedimentation rates, as follows. We
167 consider a Quaternary slip rate (Argnani and Bonazzi, 2005; Mastrolembo Ventura et al., 2014)
168 of 2 mm yr^{-1} , resulting in a subsidence rate of the hanging wall of 1.73 mm yr^{-1} . Considering a
169 sedimentation rate of $0.05\text{-}0.5 \text{ mm yr}^{-1}$ (A. Argnani, personal communication) and the smaller
170 density of sea floor sediments with regard to average crustal rocks, we correct the subsidence
171 rate to 1.7 mm yr^{-1} . We obtain scarp heights $h_1=1530$ m, $h_2=1275$ m, $h_3=850$ m at $t_1=100$ ka,
172 $t_2=250$ and $t_3=500$ ka, respectively.

173 We set up a numerical simulation for the best-constrained, latest phase of Hyblean
174 volcanism (Profile 2, Fig. 4) following the general lines used for Etna. However, the bathymetry
175 corresponding to this phase of Hyblean volcanism is less constrained, as the previously used
176 Quaternary rates cannot be extrapolated for earlier periods. Therefore, we consider three
177 snapshots with height difference on the Malta Escarpment of 500, 1500 and 2000 m (the current
178 height difference at the latitude of the Hyblean foreland is ~ 2400 m) and width of 3, 9 and 12 km
179 (preserving the current slope), that we associate to three earlier phases in the development of the
180 Malta Escarpment.

181

182 4. SIMULATIONS FOR DIKE PATHWAYS

183 The load gradient exerted by the bathymetry of the Malta Escarpment rotates the
184 principal stresses and produces curved dike trajectories in section view, linking the observed
185 volcanism (orange triangles at the surface, $x=x_{vol}$, in Figs. 3 and 4) to melt sources (orange-filled
186 dikes at 30 km depth, $x=x_{mag}$) offset to the east, below the Malta Escarpment. The bending of the
187 dike trajectories depends non-linearly on the competition between decompression (due to the
188 activity of the fault, or scarp height) and tectonic stress, as illustrated below.

189 For the tectonic extension $\sigma^T = 5$ MPa, the simulations link the ~100 ka old ($h_1=1530$ m)
190 volcanism at Etna (orange triangles at $-25 \text{ km} < x_{vol} < 5 \text{ km}$), to a source of magma located at -
191 $20 < x_{mag} < 5$ (orange-filled dikes), slightly to the west of the Malta Escarpment zone (Fig. 3a). A
192 direct link to a source below the Malta Escarpment requires a weaker tectonic extension ($\sigma^T = 1$
193 MPa), that results in $-15 \text{ km} < x_{mag} < 10 \text{ km}$ (Fig. 3d). At ~250 ka ($h_2=1275$ m), the observed
194 volcanism ($-10 \text{ km} < x_{vol} < 0 \text{ km}$) is backtracked to $0 \text{ km} < x_{mag} < 15 \text{ km}$, below the Malta
195 Escarpment, for $\sigma^T = 5$ MPa (Fig. 3b). At 500 ka ($h_3=850$ m), for $\sigma^T = 5$ MPa the
196 subaerial/submarine volcanic activity ($-5 \text{ km} < x_{vol} < 5 \text{ km}$) is again linked directly to a magma
197 source below the Malta Escarpment, at $0 \text{ km} < x_{mag} < 20 \text{ km}$.

198 Similarly to Etna, our simulations for the Hyblean region show that dikes nucleated below the
199 Malta Escarpment are deviated westwards and intersect the surface on the footwall (Fig. 4). An
200 extensional tectonic stress cannot explain the last phase of Hyblean volcanism (Fig. 4a), but a
201 compressional tectonic stress with $\sigma^T = -5$ MPa reproduces the observed distal fissures
202 perpendicular to the Malta Escarpment (Fig. 2, orange fissures). In fact, σ_3 is here out of plane
203 (Fig. 4d) and NNW-SSE trending dikes are expected to twist by 90° , intersecting the surface as
204 ENE-WSW trending fissures. Extensional stresses are however consistent with the earlier phases
205 (Fig. 2, cyan and purple fissures) of the Hyblean volcanism, with Malta Escarpment-parallel

206 fissures closer to the coast (Fig. 4b, c).

207 Distal arrivals require weaker extension (in the younger Etna case) or compression (in the
208 younger Hyblean case) (Fig. 5). The ratio of tectonic extension to decompression, σ^T/P^U
209 $=\sigma^T/(\Delta\rho gh)$, controls the bending (rotation around a ~N-S axis) of the pathways and the twisting
210 (rotation around an axis parallel to the dike propagation direction) of the dikes.

211 If a positive (extensional) σ^T dominates over P^U the trajectories are nearly vertical and
212 offset from the Malta Escarpment only by a few km. If P^U dominates, or σ^T is negative
213 (compressional), the trajectories become inclined or even sub-horizontal, inhibiting the upward
214 propagation of magma, as in the trajectories terminating at depth (see black crosses in Fig. 4d-e-
215 f). If the ratio is such that σ_3 becomes out-of-plane, then dikes are expected to twist and become
216 orthogonal to the Malta Escarpment. Therefore, depending on the σ^T/P^U value, the location of the
217 ascent of magma may be promoted or not, the pathways may change from subvertical to
218 subhorizontal, and the surface fissures may be parallel or perpendicular to the Malta Escarpment.

219 5. A COMPREHENSIVE MODEL

220 Our results show that both the Hyblean and early Etnean magma pathways dip towards
221 the Malta Escarpment. For the Etnean case, we locate the 30 km deep magma storage zone
222 inferred from petrology directly below the Malta Escarpment (Fig. 6a-c). For the Hyblean case,
223 arresting our analysis at Moho level does not allow us to reach the inferred melt generation zone
224 (between 30 and 80 km; Beccaluva et al., 1998; Klemme and O'Neill, 2000). Still, we find
225 Hyblean crustal magma pathways to follow the same overall picture of the Etnean pathways
226 (Fig. 6d-f). A melt generation zone below the Malta Escarpment may thus explain both the
227 Hyblean and Etnean volcanism, provided an appropriate amount of regional extension or
228 compression is coupled to the crustal decompression due to the deepening of the seafloor
229 induced by the activity of the Malta Escarpment. Indeed, deepening of the Malta Escarpment
230 alone is not sufficient to explain the recent volcanism in eastern Sicily. In fact, a switch from

231 extension to compression for the most recent Hyblean phase and at least a weakening of
232 extension over the lifetime of the Etnean volcanism are both needed to explain the location,
233 migration and preferred orientation of volcanism. Tectonic studies support our models, showing
234 that the modelled extension and the compression coexisted during the Etnean and Hyblean
235 volcanism, respectively (Ghisetti and Vezzani, 1980; Grasso et al., 1991; Monaco et al., 1997;
236 Beccaluva et al., 1998; Catalano et al., 2008; Cultrera et al., 2015). The weakening of the ~E-W
237 extension in the Etna area may be explained by the repeated emplacement of ~N-S trending
238 dikes, which may even create a local and/or transient compressive stress field (Vigneresse et al.,
239 1999).

240 Besides being mechanically plausible, the hypothesis of the Hyblean and Etnean magma
241 sourced below the Malta Escarpment is consistent with previous petrological models of the
242 Hyblean volcanism (Beccaluva et al., 1998; Schiano et al., 2001; Manuella et al., 2013). Indeed,
243 Hyblean magmas are relatively undifferentiated, even though lavas cover a large serial affinities,
244 varying from quartz-tholeiites, to alkaline basalts up to nephelinites (Manuella et al., 2015). This
245 wide compositional range results from different degrees of partial melting of a metasomatized
246 mantle (Scribano et al., 2009; Viccaro and Zuccarello, 2017); major and trace element contents
247 are compatible with source depths within spinel peridotite facies lithospheric mantle between 30
248 and 80 km (Beccaluva et al., 1998; Klemme and O'Neill, 2000).

249 Our models cannot help constraining the depth of magma generation or magma stalling,
250 nor the time spent by the magma at different depths. However, by following the magma
251 trajectories they return from the surface down to 30 km, which is the deepest we can go with an
252 elastic model, we have proved mechanical consistency of melt generation below the Malta
253 Escarpment rather than directly below Etna. Finally, even if we cannot reach the depth of magma
254 generation for the source feeding the Hyblean volcanism, we still find magma trajectories
255 through the crust to head for the same direction as for Etna, below the Malta Escarpment (Figs.
256 3, 4 and 6).

257 We should also note that in the Etna case, mainly a composite volcano made of
258 trachybasalts and trachyandesites, we expect a differentiation from a magma reservoir;
259 conversely, in the Hyblean case the fissure-fed tholeiitic and alkali basalts have virtually no
260 trend of differentiation. These features imply a different feeding system, with a major magmatic
261 reservoir for Etna, probably minor or absent beneath the Hyblean area. Based on our model, it is
262 difficult to put constraints on the development of a magmatic reservoir at the crust-mantle
263 boundary, as this may depend upon different factors beside stress, most importantly the supply
264 rate of magma, its density and viscosity. The higher magmatic supply beneath Etna may
265 originate from other regional processes, including the retreat of the subducting Ionian slab
266 (Gvirtzman and Nur, 1999; Clocchiatti et al., 2004; Faccenna et al., 2011).

267 In this frame, the overall northward migration of volcanism in eastern Sicily and its
268 spatial continuity may also be related to the progressive increase in the melt production due to
269 the gradual and northward deepening (or increase in the morphological scarp) of the Malta
270 Escarpment (ME).

271 Based on our simulations, we propose that the distribution and migration of volcanism in
272 eastern Sicily stems from the combination of evolving topographic loads and decompressions
273 and regional stresses varying from compressive to extensional. This study highlights the
274 potential of associating mechanically consistent magma pathways to melting source hypotheses,
275 in order to achieve better constraints on the origin of magmatism. While petrological studies can
276 provide information on the depth of a melt source, here we provide a novel method to
277 reconstruct its lateral position at depth. This method could be used on other complex cases to
278 constrain the actual horizontal location of a melt source at the depth indicated by petrological
279 evidences.

280 More generally, a comparative stress analysis may be often needed to properly explain intraplate
281 magmatism. In our case, while the source of magmatism may be explained by decompression
282 due to the thinning of the passive margin of the Malta Escarpment, the propagation path of the

283 magma may be ascribed to the intraplate evolution of these stresses and the
284 topographic/bathymetric configuration of the crust. The evolution of magmatic provinces in
285 eastern Sicily provides an outstanding example of how crustal magma transport processes over
286 time scales of millions of years, should be addressed considering both regional, tectonic
287 paleostresses, and the contribution of surface loads and their variations. Such a combination of
288 tectonic and loading stresses has so far explained several magmatic features of relatively simple
289 and general tectonic settings, as narrow rifts, calderas or sector collapses of volcanic edifices
290 (e.g., Maccaferri et al, 2011; Corbi et al., 2015; Maccaferri et al., 2017). In this study we show
291 how we can extend our approach to specific and more complex tectonic contexts, characterized
292 by both tectonic and topographic variations. We suggest that our approach can be applied to
293 other areas worldwide, where a better understanding and definition of the evolution of the
294 tectonic processes and surface elevation may help explain similar apparently enigmatic intraplate
295 volcanism.

296 **ACKNOWLEDGEMENTS**

297 F.M. and E.R. received funding from the European Union, Grant N. 308665, project MEDSUV.
298 A. Argnani provided expert and helpful advice on the Malta Escarpment. S. Conway improved
299 the English.

300

301 **REFERENCES CITED**

- 302 Argnani, A., and Bonazzi, C., 2005, Tectonics of Eastern Sicily offshore: *Tectonics*, 24,
303 doi:10.1029/2004TC001656 TC4009.
- 304 Barberi, F., Gasparini, P., Innocenti, F., and Villari, L., 1973, Volcanism of the Southern
305 Tyrrhenian Sea and its Geodynamical Implications: *J. Geophys. Res.*, 78, p. 5221–5232.
- 306 Beccaluva, L., Siena, F., Coltorti, M., Di Grande, A., Lo Giudice, A., Macciotta, G., Tassinari,
307 R., and Vaccaro, C., 1998, Nephelinitic to tholeiitic magma generation in a transtensional
308 tectonic setting: An integrated model for the Iblean volcanism, Sicily: *J. Petrol.*, 39, p.
309 1547– 1576.
- 310 Billi, A., Presti, D., Orecchio, B., Faccenna, C., and Neri, G., 2010, Incipient extension along
311 the active convergent margin of Nubia in Sicily, Italy: Cefalù-Etna seismic zone:
312 *Tectonics*, 29, TC4026, 10.1029/2009TC002559.
- 313 Branca, S., Coltelli, M., Groppelli, G., and Lentini, F., 2011, Geological map of Etna volcano,
314 1:50,000 scale: *Ital. J. Geosci.*, 130, p. 265–291, doi: 10.3301/IJG.2011.15.
- 315 Carbone, S., Grasso, M., and Lentini, F., 1987, Lineamenti geologici del Plateau Ibleo (Sicilia
316 SE): presentazione delle carte geologiche della Sicilia Sud-Orientale: *Mem. Soc. Geol. It.*,
317 38, p. 127–135.
- 318 Catalano, S., Bonforte, A., Guglielmino, F., Romagnoli, G., Tarsia, C., and Tortorici, G. 2013,
319 The influence of erosional processes on the visibility of Permanent Scatterers Features
320 from SAR remote sensing on Mount Etna (E Sicily): *Geomorphology*, 198, 128-137,
321 10.1016/j.geomorph.2013.05.020.
- 322 Catalano, S., De Guidi, G., Romagnoli, G., Torrisi, S., Tortorici, G., and Tortorici, L., 2008, The
323 migration of plate boundaries in SE Sicily: influence on the large-scale kinematic model of
324 the African promontory in southern Italy: *Tectonophysics*, 449, p. 41–62.
- 325 Chiocci, F.L., Coltelli, M., Bosmanba A., and Cavallaro, D, 2011, Continental margin large-
326 scale instability controlling the flank sliding of Etna volcano: *Earth Planet. Sci. Lett.*, 305,

327 57-64, doi:10.1016/j.epsl.2011.02.040.

328 Clocchiatti, R., Condomines, M., Guénot, N., Tanguy, J.C., 2004, Magma changes at Mount
329 Etna: the 2001 and 2002-2003 eruptions, *Earth Planet. Sci. Lett.*, 226, 397-414.

330 Corbi, F., Rivalta, E., Pinel, V., Maccaferri, F., Bagnardi, M., and Acocella, V., 2015, How
331 caldera collapse shapes the shallow emplacement and transfer of magma in active
332 volcanoes. *Earth Plan. Sci. Lett.*, 431, 287-293.

333 Corsaro, R.A., Neri, M., and Pompilio, M., 2002, Paleo-environmental and volcano-tectonic
334 evolution of the south-eastern flank of Mt. Etna during the last 225 ka inferred from
335 volcanic succession of the «Timpe», Acireale, Sicily: *J. Volcanol. Geotherm. Res.*, 113, p.
336 289-306, doi:10.1016/S0377-0273(01)00262-1.

337 Cultrera, F., Barreca, G., Scarfi, L., and Monaco, C., 2015, Fault reactivation by stress pattern
338 reorganization in the Hyblean foreland domain of SE Sicily (Italy) and seismotectonic
339 implications: *Tectonophysics*, 661, p. 215-228.

340 Dahm, T., 2000, Numerical simulations of the propagation path and the arrest of fluid-filled
341 fractures in the Earth: *Geophys. J. Int.*, 141, p. 623–638.

342 Davis, R., and Selvadurai, A., 1996, *Elasticity and Geomechanics* (Cambridge Univ. Press,
343 1996).

344 Doglioni, C., Innocenti, F., and Mariotti, G., 2001, Why Mt Etna?: *Terra Nova*, 13(1), p. 25–31,
345 doi:10.1046/j.1365-3121.2001.00301.x.

346 Faccenna, C., Molin, P., Orecchio, B., Olivetti, V., Bellier, O., Funicello, F., Minelli, L.,
347 Piromallo, C., and Billi, A., 2011, Topography of the Calabria subduction zone (southern
348 Italy): clues for the origin of Mt. Etna: *Tectonics*, 30, TC1003,
349 doi:10.1029/2010TC002694

350 Gvirtzman, Z., and Nur, A., 1999, The formation of Mount Etna as the consequence of slab
351 rollback: *Nature*, 401, p. 782–785, doi:10.1038/44555.

352 Finetti, I., 1982, Structure, stratigraphy and evolution of Central Mediterranean. *Boll. Geof.*

353 Teor. Appl., XXVI, 96, 247-312.

354 Ghisetti, F., and Vezzani, L., 1980, The structural features of the Iblean plateau and of the Monte
355 Iudica area (South Eastern Sicily): A microtectonic contribution to the deformational
356 history of the Calabrian Arc., *Boll. Soc. Geol. It.*, 99, p. 57–102.

357 Grasso, M., Pezzino, A., Reuther, C.D., Lanza, R., and Miletto, M., 1991, Late Cretaceous and
358 Recent tectonic stress orientations recorded by basalt dykes at Capo Passero (southeastern
359 Sicily): *Tectonophysics*, 185, p. 247-259.

360 Klemme, S., and O'Neill, H., 2000, The near-solidus transition from garnet lherzolite to spinel
361 lherzolite: *Contrib. Mineral. Petrol.*, 138, p. 237-248, doi:10.1007/s004100050560.

362 Lanzafame, G., Leonardi, A., Neri, M., and Rust, D., 1997, Late overthrust of the Appenine -
363 Maghrebian Chain at the NE periphery of Mt. Etna, Sicily: *C. R. Acad. Sci. Paris*, t.324,
364 serie II a, p. 325-332.

365 Maccaferri, F., Bonafede, M., and Rivalta, E., 2011, A quantitative study of the mechanisms
366 governing dike propagation, dike arrest and sill formation: *J. Volcanol. Geotherm. Res.*,
367 208, p. 39–50.

368 Maccaferri, F., Richter, N., Walter, T.R., 2017, The effect of giant lateral collapses on magma
369 pathways and the location of volcanism. *Nature Communications*, 8, 1097, DOI:
370 10.1038/s41467-017-01256-2.

371 Maccaferri, F., Rivalta, E., Keir, D., and Acocella, V., 2014, Off-rift volcanism in rift zones
372 determined by crustal unloading: *Nature Geoscience*, 7, p. 297-300.

373 Manuella, F.C., Brancato, A., Carbone, S., and Gresta, S., 2013, A crustal–upper mantle model
374 for southeastern Sicily (Italy) from the integration of petrologic and geo-physical data: *J.*
375 *Geodyn.*, 66, p. 92–102.

376 Mastrolembo Ventura, B., Serpelloni, E., Argnani, A., Bonforte, A., Bürgmann, R., Anzidei, M.,
377 Baldi, P., and Puglisi, G., 2014, Fast geodetic strain-rates in eastern Sicily (southern Italy):
378 new insights into block tectonics and seismic potential in the area of the great 1693

379 earthquake: *Earth Planet. Sci. Lett.*, 404, p. 77–88, doi:10.1016/j.epsl.2014.07.025.

380 Mattia, M., Bruno, V., Caltabiano, T., Cannata, A., Cannavò, F., D'Alessandro, W., Di Grazia,
381 G., Federico, C., Giammanco, S., La Spina, A., Liuzzo, M., Longo, M., Monaco, C.,
382 Patanè, D., and Salerno, G., 2015, A comprehensive interpretative model of slow slip
383 events on Mt. Etna's eastern flank, *Geochem. Geophys. Geosyst.*, 16, 635-658,
384 doi:10.1002/2014GC005585.

385 Monaco, C., Tapponnier, P., Tortorici, L., and Gillot, P.Y., 1997, Late Quaternary slip rates on
386 the Acireale–Piedimonte normal faults and tectonic origin of Mt. Etna (Sicily): *Earth*
387 *Planet. Sci. Lett.*, 147, p. 125–139, doi:10.1016/S0012-821X(97)00005-8.

388 Montone, P., Mariucci, M.T., and Pierdominici, S., 2012,, The Italian present-day stress map:
389 *Geophys. J. Intern.*, 189, p. 705-716.

390 Morelli, C., Gantar, C., and Pisani, M., 1975, Bathymetry, gravity and magnetism in the Strait of
391 Sicily and in the Ionian Sea. *Boll. Geof. Teor. Appl.*, 17: 39-58.

392 Niu, Y., Wilson, M., Humphreyes, E.R., and O'Hara, M., 2011, The Origin of Intra-plate Ocean
393 Island Basalts (OIB): the Lid Effect and its Geodynamic Implications: *J. Petrol.* 52, p.
394 1443-1468, doi: 10.1093/petrology/egr030.

395 Patacca, E., Scandone, P., Giunta, G., and Liguori, V., 1979, Mesozoic paleotectonic evolution
396 of the Ragusa zone (southern Sicily): *Geologica Romana*, 18, p. 331–369.

397 Polonia, A., Torelli, L., Artoni, A., Carlini, M., Faccenna, C., Ferranti, L., Gasperini, L., Govers,
398 R., Klaeschen, D., Monaco, C., Neri, G., Nijholt, N., Orecchio, B., and Wortel, R.,2016,
399 The Ionian and Alfeo - Etna fault zones: New segments of an evolving plate boundary in
400 the central Mediterranean sea?: *Tectonophysics*, 675, p. 69-90
401 doi:10.1016/j.tecto.2016.03.016.

402 Roman, A., and Jaupart, C., 2014, The impact of a volcanic edifice on intrusive and eruptive
403 activity: *Earth Planet. Sci. Lett.*, 408, p. 1-8, doi:10.1016/j.epsl.2014.09.016.

404 Rubin, A., 1995, Propagation of magma-filled cracks: *Annu. Rev. Earth Planet. Sci.*, 23, p. 287–

405 336.

406 Schiano, P., Clocchiatti, R., Ottolini, L., and Busà, T., 2001, Transition of Mount Etna lavas
407 from a mantle-plume to an island-arc magmatic source: *Nature*, 412, p. 900–904.

408 Schellart, W. P., 2010, Mount Etna-Iblean volcanism caused by rollback-induced upper mantle
409 upwelling around the Ionian slab edge: An alternative to the plume model: *Geology*, 38, p.
410 691-694.

411 Scribano, V., Viccaro, M., Cristofolini, R., Ottolini, L., 2009, Metasomatic events recorded in
412 ultramafic xenoliths from the Hyblean area (Southern Sicily, Italy). *Miner. Petrol.* 95, 235-
413 250.

414 Shabanian, E., Acocella, V., Gioncada, A., Ghasemi, H., and Bellier, O., 2012, Structural control
415 on magmatism in intraplate collisional settings: extinct example from NE Iran and current
416 analogues: *Tectonics*, 31, TC3013, doi: 10.1029/2011TC003042.

417 Sigmundsson, F., et al. 2015, Segmented lateral dyke growth in a rifting event at Bárðarbunga
418 volcanic system, Iceland: *Nature*, 517(7533), p. 191–195, doi:10.1038/nature14111.

419 Siniscalchi, A., Tripaldi, S., Neri, M., Balasco, M., Romano, G., Ruch, J., and Schiavone, D.,
420 2012, Flank instability structure of Mt Etna inferred by a magnetotelluric survey: *J.*
421 *Geophys. Res.*, 117, B03216, doi:10.1029/2011JB008657.

422 Tang, J., Obayashi, M., Niu, F., Grand, S.P., Chen, Y.J., Kawakatsu, H., Tanaka, S., Ning, J.,
423 and Ni, J.F., 2014, Changbaishan volcanism in northeast China linked to subduction-
424 induced mantle upwelling: *Nature Geoscience*, 7, p. 470-475.

425 Tanguy J.C., Condomines M., and Kieffer, G., 1997, Evolution of the Mount Etna magma:
426 Constraints on the present feeding system and eruptive mechanism: *J. Volcanol. Geotherm.*
427 *Res.*, 75, 3-4, p. 221–250.

428 Tarquini, S., Isola, I., Favalli, M., Mazzarini, F., Bisson, M., Pareschi, M. T., and Boschi, E.,
429 2007, TINITALY/01: a new Triangular Irregular Network of Italy: *Ann. Geophys.*, 50, p.
430 407 – 425.

431 Torelli, L., Grasso, M., Mazzoldi, G., and Peis, D., 1998, Plio–Quaternary tectonic evolution and
432 structure of the Catania foredeep, the northern Hyblean Plateau and the Ionian shelf (SE
433 Sicily): *Tectonophysics*, 298, p. 209–221.

434 Viccaro, M., and Zuccarello, F., 2017, Mantle ingredients for making the fingerprint of Etna
435 alkaline magmas: implications for shallow partial melting within the complex geodynamic
436 framework of Eastern Sicily. *J. Geodyn.*, 109, 10-23.

437 Vigneresse, JL, Tikoff, B., and Ameglio, L., 1999, Modification of the regional stress field by
438 magma intrusion and formation of tabular granitic plutons: *Tectonophysics*, 302, p. 203-
439 224, doi:10.1016/S0040-1951(98)00285-6.

440 Watanabe, T., Masuyama, T., Nagaoka, K., and Tahara, T., 2002, Analog experiments on
441 magma-filled cracks: Competition between external stresses and internal pressure: *Earth
442 Planets Space*, 54, p. 1247–1261.

443

444

445 **FIGURE CAPTIONS**

446

447 **Figure 1. Simplified tectonic map of Sicily.** P1 and P2 (white lines) are the location of the
448 profiles illustrated in Figs. 3 and 4, respectively. The image of the Italian territory is obtained
449 from the TINITALY DEM (Tarquini et al., 2007) re-sampled to 100 m resolution.

450

451 **Figure 2. Etnean and Hyblean volcanism in eastern Sicily.** Positions of eruptive centers (dots)
452 and fissures (colored lines) in eastern Sicily (see Fig. 1 for location). Volcanic outcrops are in
453 light gray. The arrows in the legend represent the more recent and better constrained direction of
454 regional extension (white) or compression (black). SG=Simeto Graben; LSG=Lentini-Scordia
455 Graben; ME=Malta Escarpment (main faults=black dotted lines). Data sources: Carbone et al.,
456 1987; Grasso et al., 1991, Lanzafame et al., 1996; Monaco et al., 1997; Beccaluva et al., 1998;
457 Corsaro et al., 2002, Branca et al., 2011.

458

459 **Figure 3. Simulations for dike path in Etnean area.** Principal stresses and simulated dike
460 pathways along the EW profile P1 (location in Fig. 1); z is depth below sea level, x is horizontal
461 coordinate along an ~E-W direction through Etna, perpendicular to the Malta Escarpment (ME).
462 The dashed profile of Etna is included as a reference (its load is not included in the stress
463 model). The left and right columns are for 5 and 1 MPa extensional stress, respectively; the
464 different rows correspond to different fault scarp heights and epochs, as indicated in the inlets.
465 Grey segments are σ_3 directions. Black curves are simulated dike pathways which link starting
466 dikes (vertical ellipses at $z=30$ km and $x=x_{\text{mag}}$) to a surface triangle ($z=0$ km, $x=x_{\text{vol}}$). Surface
467 volcanism observed in the individual epochs is indicated by orange-filled triangles; Orange
468 ellipses correspond to feeder dikes at their nucleation depth. Color shading indicates intensity of

469 isotropic stress $\sigma^I=(1+\nu)(\sigma_{xx}+\sigma_{zz})/3$ (where plane strain is assumed), resulting from the
470 combination of tectonic and unloading stresses. Stress is positive if extensional (see color bars to
471 the right). Dikes more likely reach the surface for higher extensional stresses (darker colours).
472 Parameters used are: crustal shear modulus is 20 MPa, Poisson's ratio is 0.25, rock density is
473 2600 kg m^{-3} , initial volume of the dikes is $2.5 \cdot 10^{-2} \text{ km}^3$ and magma buoyancy is 300 kg m^{-3} .

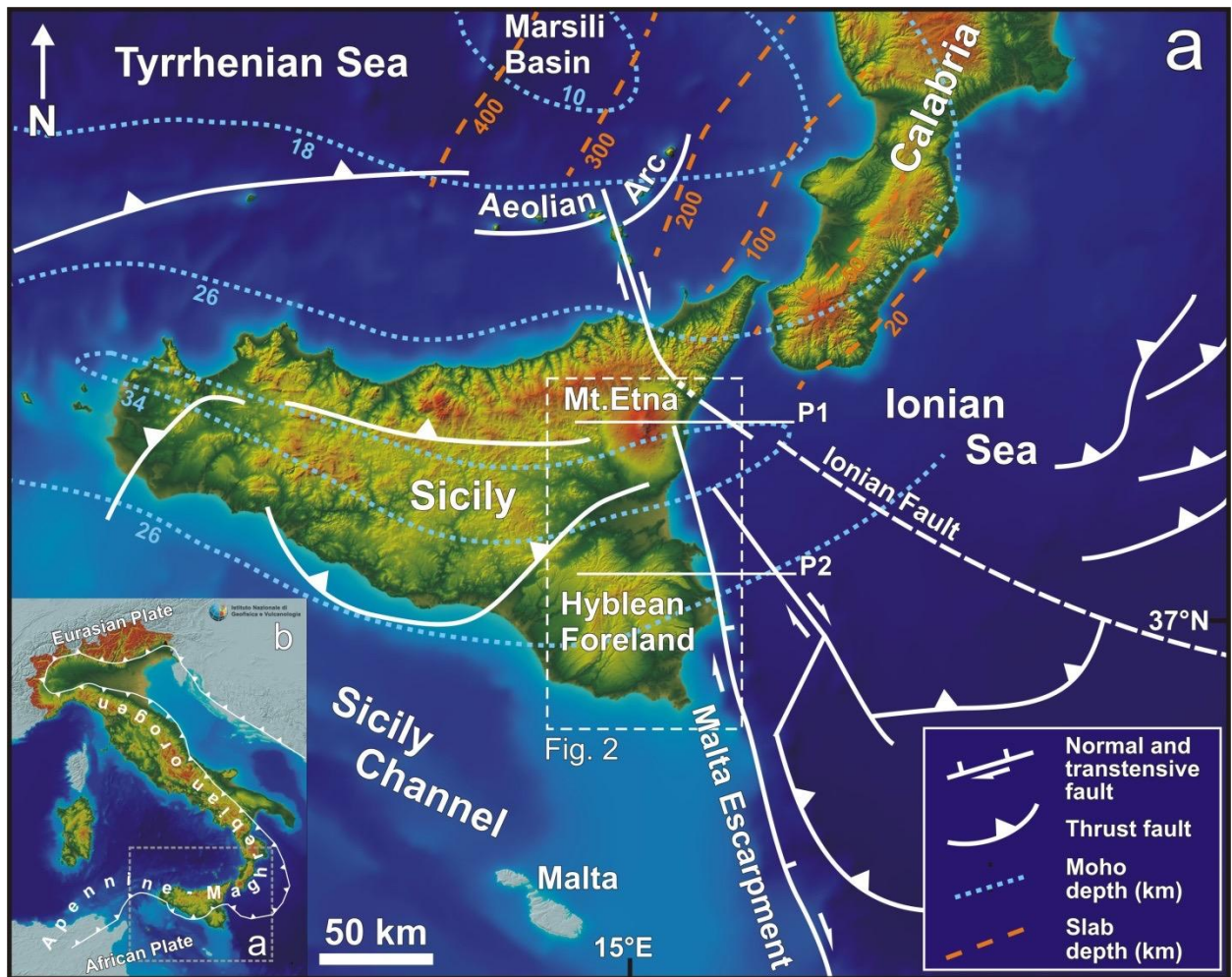
474
475 **Figure 4. Simulations for dike path in Hyblean area.** Same as Fig. 3, but relative to the ~E-W
476 profile P2 through the Hyblean foreland (location in Fig. 1). The simulation refers to the fault
477 scarp heights indicated in the inlets, developed during Upper Miocene–Lower Pleistocene (1-10
478 Ma). Grey segments are σ_3 directions; a circle indicates out of plane σ_3 (perpendicular to the
479 page), inducing dikes to twist and align to the page. Pathways of dikes that are halted on their
480 way without reaching the surface terminate with a cross (x). Color shading indicates intensity of
481 isotropic stress $\sigma^I=(1+\nu)(\sigma_{xx}+\sigma_{zz})/3$, resulting from the combination of tectonic and unloading
482 stresses. Stress is positive if extensional, negative if compressional (see color bars to the right).

483
484 **Figure 5. Migration of volcanism in eastern Sicily** due to variation of the regional tectonic
485 stresses and crustal decompression. Distance d from the Malta Escarpment of surface fissures
486 generated by dikes starting beneath the Malta Escarpment as a function of the tectonic/unloading
487 stress ratio, σ^T/P^U . Crosses indicate dikes that turned σ perpendicular to the Malta Escarpment and
488 extend laterally up to a distance d . The colored inlets on the right-hand side indicate observed
489 distances from the Malta Escarpment for surface vents in the different epochs. The colors refer to
490 those used in Fig. 2.

491
492 **Figure 6. A synthetic tectono-magmatic model for eastern Sicily.** Schematic E-W crustal
493 cross-sections below Etna (a, b, c) and the Hyblean Foreland (d, e, f), along profiles P1 and P2,

494 respectively (location in Fig. 1). In both cases, the magma storage zones are imaged at ~30 km
495 depth, i.e the starting depth of our models. Question marks show the uncertainties in the limits of
496 the magma storage regions, especially for Hyblean case. Volcanism in the Etna region has been
497 active since ~500 ka, and migrated westward under E-W and WNW-ESE tectonic extension. It
498 has been possibly fed by a larger magma storage zone below the Malta Escarpment, also
499 supplied at deeper levels from the asthenospheric window at the western edge of the subducting
500 oceanic Ionian lithosphere (not shown here). Volcanism in the Hyblean Foreland was fed by a
501 possible smaller magma storage zone located below the Malta Escarpment. Up to Miocene, dikes
502 followed NNW-SSE oriented paths (e, f), driven by ENE-WSW tectonic extension. During
503 Pliocene-Early Pleistocene (d), the tectonic regime switched to ENE-WSW compression and the
504 dike trajectories rotated towards NE-SW to E-W paths. Crustal profiles from Morelli et al.
505 (1975), and Finetti, (1982), modified.

506



508

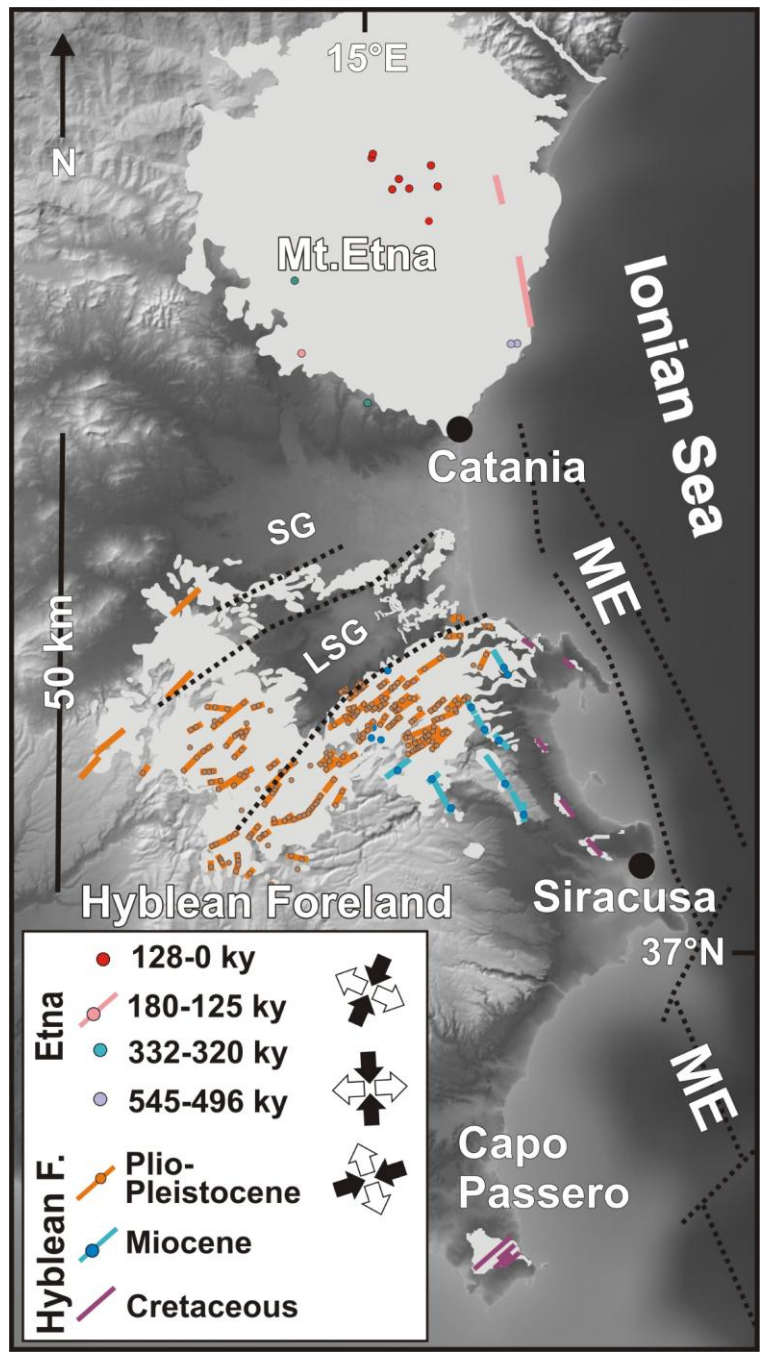
509

510 **Figure 1. Simplified tectonic map of Sicily.** P1 and P2 (white lines) are the location of the profiles
 511 illustrated in Figs. 3 and 4, respectively. The image of the Italian territory is obtained from the
 512 TINITALY DEM (Tarquini et al., 2007) re-sampled to 100 m resolution.

513

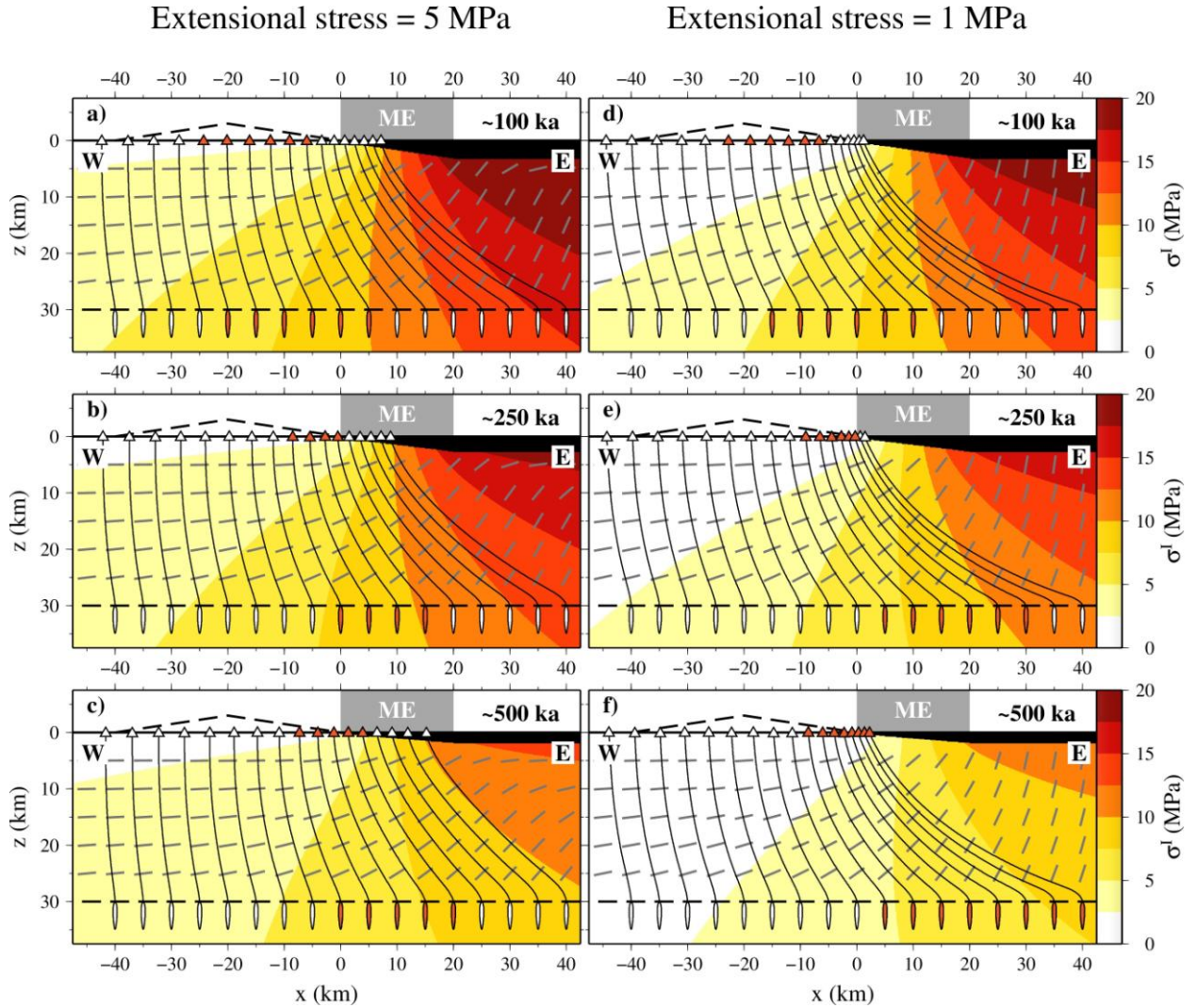
514

515
 516
 517
 518
 519
 520
 521
 522
 523
 524
 525
 526
 527
 528
 529
 530
 531
 532



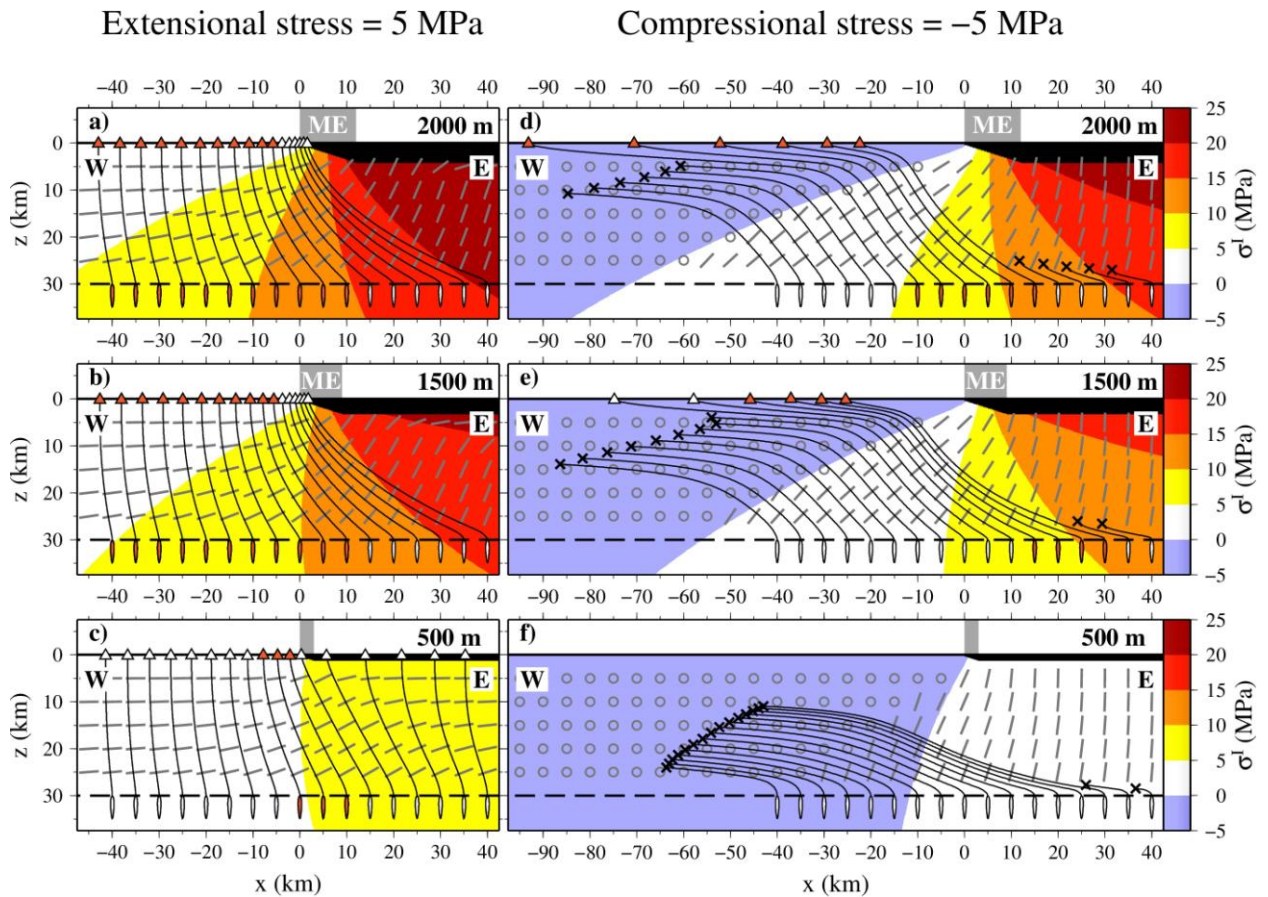
533
 534
 535
 536
 537
 538
 539
 540

Figure 2. Etnean and Hyblean volcanism in eastern Sicily. Positions of eruptive centers (dots) and fissures (colored lines) in eastern Sicily (see Fig. 1 for location). Volcanic outcrops are in light gray. The arrows in the legend represent the more recent and better constrained direction of regional extension (white) or compression (black). SG=Simeto Graben; LSG=Lentini-Scordia Graben; ME=Malta Escarpment (main faults=black dotted lines). Data sources: Carbone et al., 1987; Grasso et al., 1991, Lanzafame et al., 1996; Monaco et al., 1997; Beccaluva et al., 1998; Corsaro et al., 2002, Branca et al., 2011.



541 **Figure 3. Simulations for dike path in Etna area.** Principal stresses and simulated dike pathways
542 along the EW profile P1 (location in Fig. 1); z is depth below sea level, x is horizontal coordinate along
543 an ~E-W direction through Etna, perpendicular to the Malta Escarpment (ME). The dashed profile of
544 Etna is included as a reference (its load is not included in the stress model). The left and right columns are
545 for 5 and 1 MPa extensional stress, respectively; the different rows correspond to different fault scarp
546 heights and epochs, as indicated in the inlets. Grey segments are σ_3 directions. Black curves are simulated
547 dike pathways which link starting dikes (vertical ellipses at $z=30$ km and $x=x_{mag}$) to a surface triangle ($z=0$
548 km, $x=x_{vol}$). Surface volcanism observed in the individual epochs is indicated by orange-filled triangles;
549 Orange ellipses correspond to feeder dikes at their nucleation depth. Color shading indicates intensity of
550 isotropic stress $\sigma^I=(1+\nu)(\sigma_{xx}+\sigma_{zz})/3$ (where plane strain is assumed), resulting from the combination of
551 tectonic and unloading stresses. Stress is positive if extensional (see color bars to the right). Dikes more
552 likely reach the surface for higher extensional stresses (darker colours). Parameters used are: crustal shear
553 modulus is 20 MPa, Poisson's ratio is 0.25, rock density is 2600 kg m⁻³, initial volume of the dikes is
554 $2.5 \cdot 10^{-2}$ km³ and magma buoyancy is 300 kg m⁻³.

555



556

557

558 **Figure 4. Simulations for dike path in Hyblean area.** Same as Fig. 3, but relative to the ~E-W profile
 559 P2 through the Hyblean foreland (location in Fig. 1). The simulation refers to the fault scarp heights
 560 indicated in the inlets, developed during Upper Miocene–Lower Pleistocene (1-10 Ma). Grey segments
 561 are σ_3 directions; a circle indicates out of plane σ_3 (perpendicular to the page), inducing dikes to twist and
 562 align to the page. Pathways of dikes that are halted on their way without reaching the surface terminate
 563 with a cross (x). Color shading indicates intensity of isotropic stress $\sigma^I = (1+\nu)(\sigma_{xx} + \sigma_{zz})/3$, resulting from
 564 the combination of tectonic and unloading stresses. Stress is positive if extensional, negative if
 565 compressional (see color bars to the right).

566

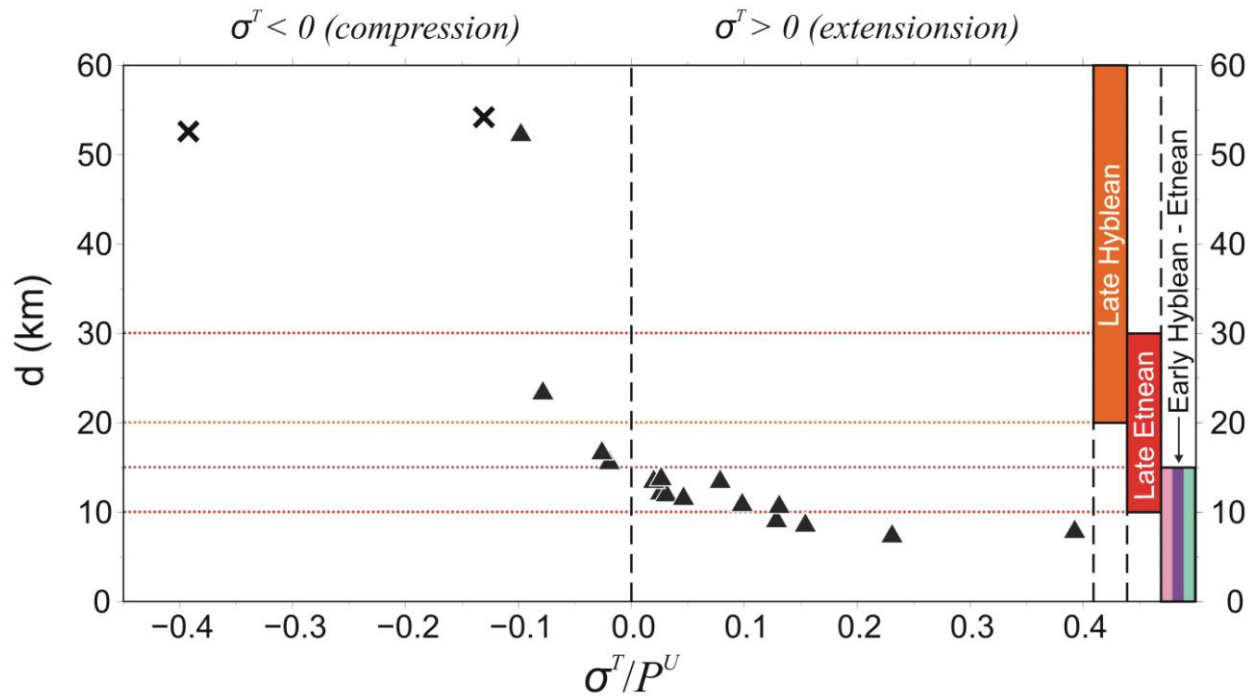
567

568

569

570

571



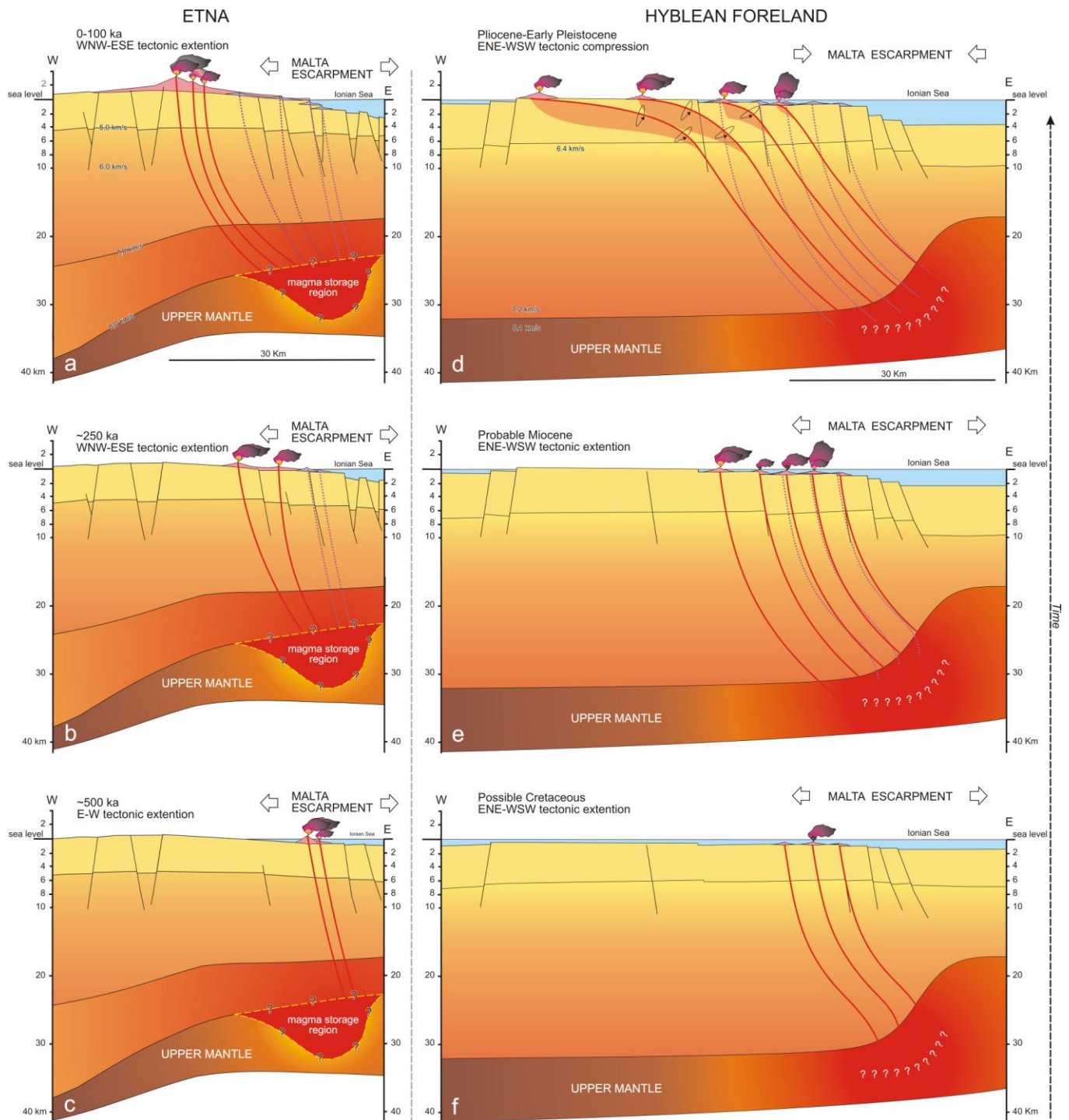
572

573

574 **Figure 5. Migration of volcanism in eastern Sicily** due to variation of the regional tectonic stresses and
575 crustal decompression. Distance d from the Malta Escarpment of surface fissures generated by dikes
576 starting beneath the Malta Escarpment as a function of the tectonic/unloading stress ratio, σ^T/P^U . Crosses
577 indicate dikes that turned perpendicular to the Malta Escarpment and extend laterally up to a distance d .
578 The colored inlets on the right-hand side indicate observed distances from the Malta Escarpment for
579 surface vents in the different epochs. The colors refer to those used in Fig. 2.

580

581



582

583 **Figure 6. A synthetic tectono-magmatic model for eastern Sicily.** Schematic E-W crustal cross-
 584 sections below Etna (a, b, c) and the Hyblean Foreland (d, e, f), along profiles P1 and P2, respectively
 585 (location in Fig. 1). In both cases, the magma storage zones are imaged at ~30 km depth, i.e the starting
 586 depth of our models. Question marks show the uncertainties in the limits of the magma storage regions,
 587 especially for Hyblean case. Volcanism in the Etna region has been active since ~500 ka, and migrated
 588 westward under E-W and WNW-ESE tectonic extension. It has been possibly fed by a larger magma
 589 storage zone below the Malta Escarpment, also supplied at deeper levels from the asthenospheric window
 590 at the western edge of the subducting oceanic Ionian lithosphere (not shown here). Volcanism in the
 591 Hyblean Foreland was fed by a possible smaller magma storage zone located below the Malta

592 Escarpment. Up to Miocene, dikes followed NNW-SSE oriented paths (e, f), driven by ENE-WSW
593 tectonic extension. During Pliocene-Early Pleistocene (d), the tectonic regime switched to ENE-WSW
594 compression and the dike trajectories rotated towards NE-SW to E-W paths. Crustal profiles from Morelli
595 et al. (1975), and Finetti, (1982), modified.

596

Figure (high-resolution)_01

[Click here to download Figure \(high-resolution\): Figure_01.jpg](#)

Figure (high-resolution)_02

[Click here to download Figure \(high-resolution\): Figure_02.jpg](#)

Figure (high-resolution)_03

[Click here to download Figure \(high-resolution\): Figure_03.jpg](#)

Figure (high-resolution)_04

[Click here to download Figure \(high-resolution\): Figure_04.jpg](#)

Figure (high-resolution)_05

[Click here to download Figure \(high-resolution\): Figure_05.jpg](#)

Figure (high-resolution)_06

[Click here to download Figure \(high-resolution\): Figure_06.jpg](#)